frontiers | Frontiers in Physics

TYPE Original Research
PUBLISHED 25 October 2024
DOI 10.3389/fphy.2024.1409318

Check for updates

OPEN ACCESS

EDITED BY
Aurang Zaib,
Federal Urdu University of Arts, Sciences and Technology Islamabad, Pakistan

REVIEWED BY
Farhan Ali,
Federal Urdu University of Arts, Sciences and Technology Islamabad, Pakistan
Muhammad Ijaz Khan,
Lebanese American University, Lebanon

*CORRESPONDENCE
Muhammad Imran,
drmimranchaudhry@gcuf.edu.pk

RECEIVED 29 March 2024
ACCEPTED 30 September 2024
PUBLISHED 25 October 2024

CITATION
Wu Y, Chaudhry M, Maqbool N, Tahir M, Basit MA and Imran M (2024) Entropy generation in radiative motion of tangent hyperbolic nanofluid in the presence of gyrotactic microorganisms and activation energy.
Front. Phys. 12:1409318.
doi: 10.3389/fphy.2024.1409318

Entropy generation in radiative motion of tangent hyperbolic nanofluid in the presence of gyrotactic microorganisms and activation energy

Yong Wu[1], Munaza Chaudhry[2], Noureen Maqbool[3], Madeeha Tahir[3], Muhammad Abdul Basit[2,4,5] and Muhammad Imran[2,6]*

[1]General Education Department, Anhui Xinhua University, Hefei, China, [2]Department of Mathematics, Government College University, Faisalabad, Pakistan, [3]Department of Mathematics, Government College Women University, Faisalabad, Pakistan, [4]Guangzhou Institute of Energy Conversion, Chinese Academy of Sciences, Guangzhou, China, [5]School of Energy Science and Engineering, University of Science and Technology of China, Guangzhou, China, [6]Department of Mathematics and Science Education, Education Faculty, Biruni University, Istanbul, Turkey

In this work, entropy generation is optimized through the application of the second law of thermodynamics. The slip mechanisms, Brownian diffusions, and thermophoresis are elaborated using the tangent hyperbolic nanomaterial model. Magnetohydrodynamic (MHD) fluid is taken into consideration. To characterize the impact of activation energy, a unique model involving the binary chemical reaction is deployed. The effects of mixed convection that is nonlinear in nature, bioconvection, and Joule effect are all taken into consideration. The key partial differential equations (PDEs) are reduced into ordinary differential equations (ODEs) by utilizing appropriate similarity transformations and then solved numerically with the help of a built-in 'bvp4c' technique of MATLAB software. Varied flow parameters' impacts on the nanoparticle volume concentration, entropy number, microorganism concentration, temperature, and velocity fields are analyzed using graphs. Various flow variables are taken into consideration to calculate the total rate of entropy generation. The obtained results show that concentration irreversibility, Joule effect irreversibility, viscous dissipation, and heat irreversibility all influence the entropy. The numerical outcomes were observed by fixing the physical parameters as $0.1 < \alpha < 4.0$, $0.1 < M < 1.2$, $0.1 < Nr < 2.2$, $0.1 < Le < 2.2$, $0.1 < Nb < 0.4$, $0.1 < Nt < 1.0$, $2.0 < \Pr < 5.0$, and $0.1 < Lb < 2.0$, as well as their impact on the momentum, thermal, concentration, and microorganism density profiles. From results, an increasing estimate of the variable representing chemical reaction indicates a decline in the concentration. The higher the chemical reaction variable, Hartmann number, and Weissenberg number, the higher the entropy number, while the Bejan number has a contrary behavior. Subsequently, all the outcomes are plotted in graphs and discussed in detail, when subjected to the involving physical quantities.

KEYWORDS

nanoparticles, magnetohydrodynamic flow, mixed convection, chemical reaction, radiation, bioconvection, inclined sheet

1 Introduction

Engineers and scientists have held a longstanding fascination with researching non-Newtonian fluids, primarily because of their behavior on stretched surfaces with heat and mass transfer. This is because of its numerous practicalities, such as paper manufacturing, wire drawing, paper manufacturing, petroleum production, and polymer sheet manufacturing. Because shear rate and shear stress are not linearly related in non-Newtonian fluids, one constitutive equation is insufficient for representing the relationship between shear rates and shear stresses. Owing to this, various frameworks have been presented in the literature, including the Maxwell model, Reiner–Rivlin model, generalized Burgers, Oldroyd-A model, Oldroyd-B model, Oldroyd-8 constants, Carreau model, and the Carreau–Yasuda model. In the current investigation, we took non-Newtonian tangent hyperbolic fluid under consideration. Effects of shear thinning are described by a four-constant pseudoplastic model of fluid, i.e., tangent hyperbolic fluid. When flow decreases, owing to increased shear stress, it is useful to evaluate the inter-particle friction in the fluid. Examples of such liquids include ketchup, paint, blood, nail polish, and whipped cream. [1] presented a numerical approach for the flow of rate-type fluid across the stretchable cylinder using MHD flow. [2] focused on thermal radiation, which is non-linear in nature, to probe the flow by a stretchable surface with Brownian diffusion and thermophoresis. The flow of the two-dimensional rate-type fluid toward a stretchable sheet with the applied magnetic effect was investigated [3]. [4] found solutions in the series form for a tangent hyperbolic fluid that is inclined uniformly in a tube. [5] analyzed the tangent hyperbolic fluid using a stretchable sheet while considering both the impacts of Soret and Dufour in MHD stagnation point flow. [6–13] provided more research articles on non-Newtonian fluids.

Recently, some energy-efficient mechanisms have been designed to minimize the quantity of wasted energy and boost energy utilization capabilities of liquid systems. The transport of heat and viscous dissipation results in energy waste, which aids the irreversibility of the liquid system. Electrochemical and chemical, evaporative cooling, natural convection, solar thermal, microchannels, air separators, chillers, gas turbines, fuel cells, and functionally graded materials are all examples of systems where entropy generation minimization (EGM) is beneficial. [14] recently analyzed the generation of entropy in nanofluids using copper and silver nanoparticles. [15] studied the increase in entropy in a burner model with various energy sources. The optimization of entropy in a nonlinear radiative flow while accounting for Joule effects and dissipation is investigated by [16].

The change in density over a region induces additive rapid movement in self-propelled microorganisms; as a result of this, there is macroscopic movement of the fluid, which is termed as bioconvection. Self-propelled microorganisms have a tendency to enhance the base fluid to create a bio-convective stream in a specific direction. The self-propelled microorganisms are categorized into different types, i.e., gyrotactic, negative gravitaxis, and chemotaxis or oxytactic microorganisms. Compared to self-propelled microorganisms, nanoparticles do not move on their own, and their movement is driven by the effect of Brownian motion and thermophoresis. If there is minimal nanoparticle concentration, then in the nanofluids, bioconvection is supposed to be feasible and it will not result in an essential increase in the thickness of the base fluid. Bioconvection with nanoparticles was originally discussed in [17, 18]. Afterward, combining nanoparticles with gyrotactic microorganisms was proposed by [19] using Buongiornos theory.[20] studied the flow of nanofluids with bioconvection in porous medium numerically. Bioconvective flow with nanoparticles through a symmetric channel was studied by [21], and a bio nanoengineering model was presented. In rapidly changing magnetic lines of force, the clot blood model was also analyzed by [22] using the Jeffrey fluid model with microorganisms and nanoparticles. A magnetized laminar flow of nanofluid along with phototactic microorganisms in a medium that is non-Darcy with pores was observed by [23]. The external magnetic effect and bioconvective flow were researched by [24] with convective boundary conditions and nanoparticles.

In the recent past, as a result of advancements in nanotechnology, the researchers' focus has shifted to improving heat transport through the nanoparticle interaction. Because of their fascinating thermo-physical aspects, the nanoparticles, which include metallic particles of micro-size, are useful in biological, mechanical, chemical, and other engineering fields. The conductivity of heat energy and the viscosity of the fluid improve not just with the addition of nanoparticles but also with the structure of particle size, and slip features in nanoparticles play an important role as well. [25] developed nanoparticles to improve the product efficiency and fluid thermal conductivity. Heat transfer near a stagnation point in the Maxwell nanofluid flow over a porous rotating disk, highlighting the impact of shear stress and flow field alterations on heat transfer, has been investigated by [26]. Some interesting studies on nanofluids have been discussed in [27–30]. [31] analyzed the magnetohydrodynamic stagnation point flow of Williamson hybrid nanofluid over a porous sheet, considering chemical reactions, energy generation, and boundary conditions. [32] examined the unsteady 2D laminar flow of Williamson hybrid nanoliquid over a convectively heated stretching sheet, focusing on maximizing energy and mass transfer rates. [33] investigated entropy generation in the mixed convection time-dependent flow of cross-hybrid nanoliquid at a stagnation point using engine oil with $CuO\ and\ TiO_2$ nanoparticles.

Activation energy and chemical reactions have been used in mass transportation phenomena, which have been carried out in the history of food sciences, chemistry, chemical, and mechanical industries. In 1889, Svante Arrhenius engaged in the key observations on activation energy and defined it in terms of the least quantity of energy that is required to begin a chemical process. Geothermal sciences, petroleum engineering applications, oil reserves, heat reactions, and a lot of other fields are part of the activation energy phenomenon. Some major contributions to this subject are discussed in [34–36]. [37] numerically investigated the natural convection boundary-layer flow over a truncated cone with gyrotactic microorganisms in water-based nanofluid, revealing enhanced transport properties and boundary conditions' effects. [38] explored the bioconvection phenomenon of a nanofluid with gyrotactic microorganisms around a horizontal circular cylinder, utilizing Buongiorno's model and finite-difference algorithm for the comprehensive analysis of transport phenomena. [39] investigated mixed convection of nanofluid with gyrotactic microorganisms over a permeable vertical surface in a porous medium, which reveals suction/injection effects, with significant impacts on heat and mass transfer. [40] also examined the mixed bio-convective stagnation

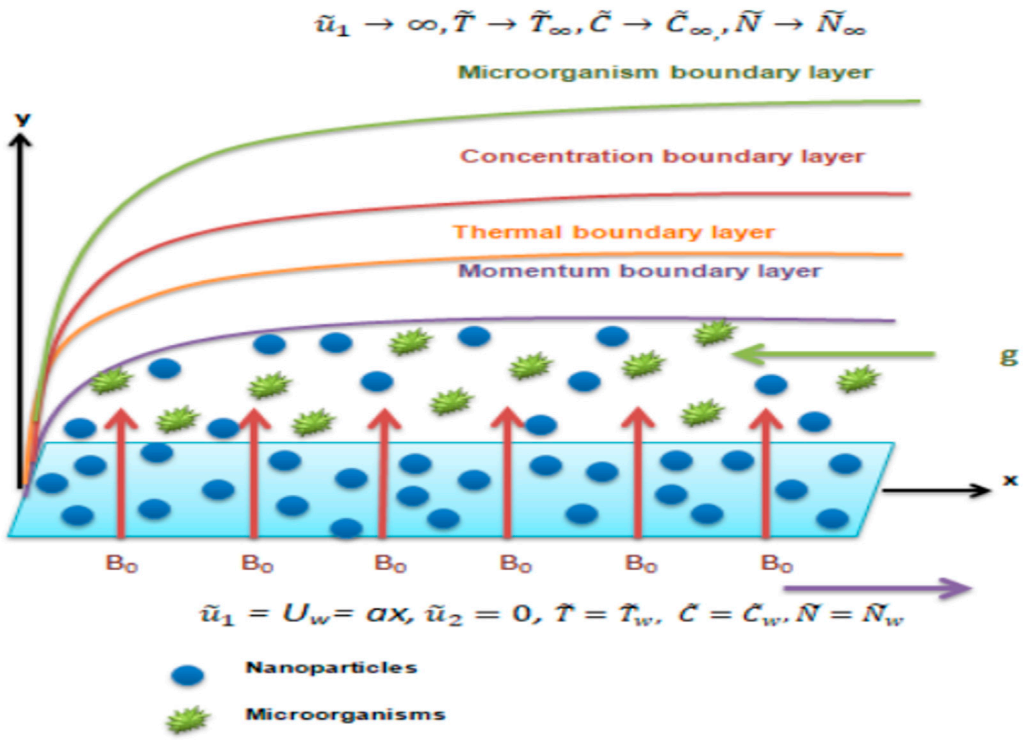

FIGURE 1
Geometrical representation of the problem.

point flow of a power-law nanofluid over a stretchable surface with passively controlled boundary conditions. [41] explored non-Newtonian nanofluid flow induced by a rotating stretchable disk, analyzing heat and mass transfer with Stefan blowing and Cattaneo–Christov fluxes. He also examined the flow of a non-Newtonian nanofluid in a conical gap between rotating/stationary surfaces, considering heat and mass transfer and a uniform magnetic field [42]. Some of the similar results are discussed in [43–45]. The study of the fluid flow in porous medium is of great importance in fluid mechanics. [46] analyzed the motion of Jeffrey nanofluid in porous medium with motile microorganisms between two revolving stretching disks. The study of different types of fluids in between porous medium is given in [47–50]. Furthermore, heat and mass transfer analysis of nanofluid is numerically scrutinized under the influence of magnetic field subject to marangoni boundary layer [51, 52].

The major goal of this work is to look at the optimization of entropy in the tangent hyperbolic nanofluid flow on a stretchable sheet. The uniqueness of the work under discussion is that it investigates the optimization of entropy generation in a non-Newtonian fluid model with non-linear thermal radiation, non-linear mixed convection, viscous dissipation, bioconvection, and activation energy as additional effects. To characterize activation energy's effects, we used a unique two-step chemical reaction model. Various flow variables are utilized to compute the rate of total entropy generation. We have used a method called the shooting technique to deal with the nonlinear ordinary system. To examine the behavior of the included variables on fluid properties, graphs and tables are created. Analysis on various methodologies is shown in [53–56].

2 Mathematical model

In tangent hyperbolic nanomaterial flow, we analyzed Bejan numbers and entropy. In the current model, the impacts of non-linear heat radiation, non-linear mixed convection, activation energy, and Joule effect are studied. The stretchable sheet with the stretching rate being a generates the flow. $\tilde{T}_w, \tilde{C}_w$, and $\tilde{N}_w$ signify the temperature, concentration, and density of self-propelling microorganisms at the sheet, respectively, while $\tilde{T}_\infty, \tilde{C}_\infty$, and $\tilde{N}_\infty$ represent the ambient temperature, concentration, and density of self-propelling microorganisms, respectively. B_0 magnetic strength is in the y-direction (see Figure 1). In light of these considerations, the governing equations for the given problem are Equations 1–6 [57]:

$$\frac{\partial \tilde{u}_1}{\partial x} + \frac{\partial \tilde{u}_2}{\partial y} = 0, \quad (1)$$

$$\begin{aligned}\tilde{u}_1 \frac{\partial \tilde{u}_1}{\partial x} + \tilde{u}_2 \frac{\partial \tilde{u}_1}{\partial y} &= \frac{\partial^2 \tilde{u}_1}{\partial y^2} \nu (1-s) + \frac{\partial \tilde{u}_1}{\partial y} \frac{\partial^2 \tilde{u}_1}{\partial y^2} \sqrt{2} \nu s \Gamma - \frac{\sigma}{\rho_f} {B_0}^2 \tilde{u}_1 \\ &+ g\beta (1 - C_\infty)(\tilde{T} - \tilde{T}_\infty) - g\left(\frac{\rho_m - \rho_f}{\rho_f}\right) \\ &\times (\tilde{C} - \tilde{C}_\infty) - \gamma_1 g \left(\frac{\rho_m - \rho_f}{\rho_f}\right)(\tilde{N} - \tilde{N}_\infty), \quad (2)\end{aligned}$$

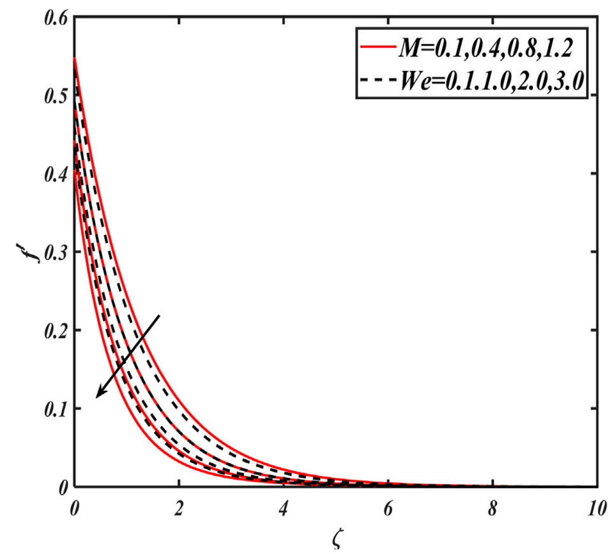

FIGURE 2
Illustration of M and We on f'.

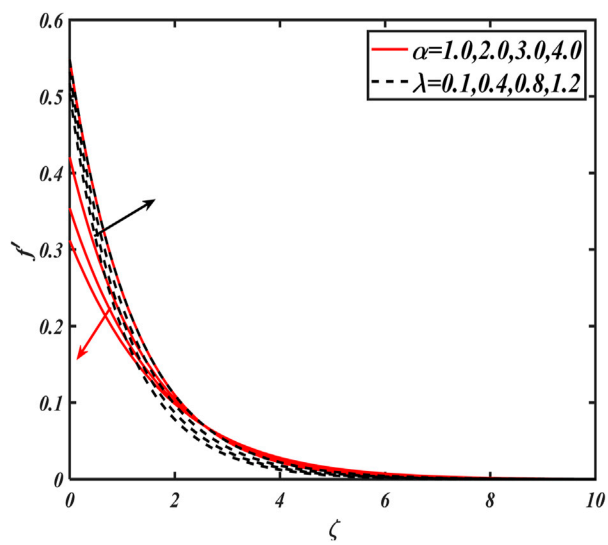

FIGURE 3
Illustration of α and λ on f'.

$$\tilde{u}_1 \frac{\partial \tilde{T}}{\partial x} + \tilde{u}_2 \frac{\partial \tilde{T}}{\partial y} = \frac{\partial^2 \tilde{T}}{\partial y^2}\frac{k}{(\rho c_p)_f} + \left\{ D_B \frac{\partial \tilde{C}}{\partial y}\frac{\partial \tilde{C}}{\partial y} + \frac{D_T}{\tilde{T}_\infty}\left(\frac{\partial \tilde{T}}{\partial y}\right)^2\right\}\frac{(\rho c_p)_s}{(\rho c_p)_f} + \left[3\tilde{T}^2 \left(\frac{\partial \tilde{T}}{\partial y}\right)^2 + \tilde{T}^3 \frac{\partial^2 \tilde{T}}{\partial y^2}\right]\times \frac{1}{(\rho c_p)_f}\frac{16\sigma^*}{3k^*} + \frac{\sigma}{(\rho c_p)_f}B_0^2 \tilde{u}_1^2 + \left(\frac{\partial \tilde{u}_1}{\partial y}\right)^2 \frac{\mu}{(\rho c_p)_f}(1-s) + \frac{\partial \tilde{u}_1}{\partial y}\left(\frac{\partial \tilde{u}_1}{\partial y}\right)^2 \times \frac{s\mu\Gamma}{(\rho c_p)_f\sqrt{2}}, \tag{3}$$

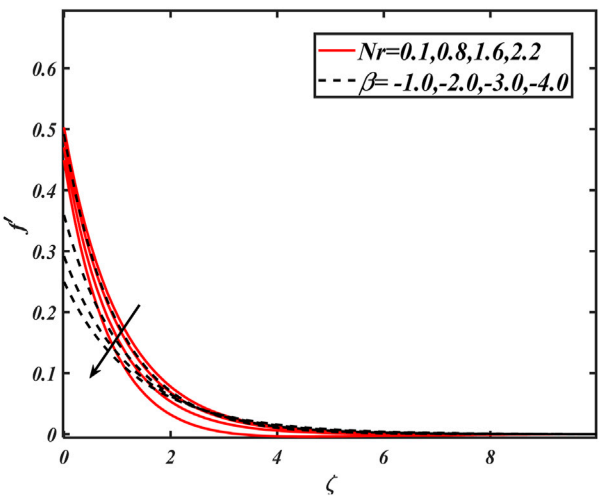

FIGURE 4
Illustration of Nr and β on f'.

$$\tilde{u}_1 \frac{\partial \tilde{C}}{\partial x} + \tilde{u}_2 \frac{\partial \tilde{C}}{\partial y} = \frac{\partial^2 \tilde{C}}{\partial y^2} D_B + \frac{\partial^2 \tilde{T}}{\partial y^2}\frac{D_T}{\tilde{T}_\infty} - k_r^{\,2}\left(\frac{\tilde{T}}{\tilde{T}_\infty}\right)^n exp\left[\frac{-E_a}{\kappa \tilde{T}}\right] \times \left(\tilde{C}_w - \tilde{C}_\infty\right), \tag{4}$$

$$\tilde{u}_1 \frac{\partial \tilde{N}}{\partial x} + \tilde{u}_2 \frac{\partial \tilde{N}}{\partial y} + \frac{bW_c}{\left(\tilde{C} - \tilde{C}_\infty\right)}\left[\frac{\partial}{\partial y}\left(\tilde{N}\frac{\partial \tilde{C}}{\partial y}\right)\right] = D_m\left(\frac{\partial^2 \tilde{N}}{\partial y^2}\right). \tag{5}$$

Following are the flow constraints used with the current flow model:

$$\begin{aligned} &\tilde{u}_1 = U_w = ax, \tilde{u}_2 = 0, \tilde{T} = \tilde{T}_w, \tilde{C} = \tilde{C}_w, \tilde{N} = \tilde{N}_w \ at \ y = 0,\\ &\tilde{u} \to 0, T \to T_\infty, C \to C_\infty, N \to N_\infty as \ y \to \infty, \end{aligned} \tag{6}$$

where $(\tilde{u}_1, \tilde{u}_2)$ denote the velocity in the (x, y) direction, respectively; (s) being power law index, (ν) is the kinematic viscosity, (Γ) is notified as the Williamson parameter, (σ) denotes the electrical conductivity, (ρ_f) represents the density of the fluid, (C_p) is the specific heat, $(\tilde{T})$ is the temperature of the fluid, (σ^*) represents the Stefan–Boltzmann constant, (μ) is the dynamic viscosity, (k^*) is the coefficient of mean absorption, (D_B) is the coefficient of Brownian diffusion, (k) is the thermal conductivity, (D_T) represents the coefficient of thermophoretic diffusion, $(k_r^{\,2})$ is the chemical reaction rate constant (n) denotes the fitted rate constants, $(\tilde{C})$ is the fluid concentration, (E_a) is activation energy, $\kappa = 8.61105\ eV/K$ is the Boltzmann constant, $((\frac{\tilde{T}}{\tilde{T}_\infty})^n exp[\frac{E_a}{\kappa \tilde{T}}])$ represents the modified Arrhenius parameter, $(\tilde{N})$ is the microorganism concentration, (D_m) shows the diffusion coefficient of microorganisms, (b) denotes the chemotaxis constant, and (W_c) is the maximum swimming speed of cell.

For present flow, suitable transformations Equation 7 are derived from [53]

$$\begin{aligned} &\xi = \sqrt{\frac{a}{\nu}}, \tilde{u}_1 = axf'(\xi), \tilde{u}_2 = -\sqrt{a\nu} f(\xi), \theta = \frac{\tilde{T} - \tilde{T}_\infty}{\tilde{T}_w - \tilde{T}_\infty},\\ &\phi = \frac{\tilde{C} - \tilde{C}_\infty}{\tilde{C}_w - \tilde{C}_\infty}, \chi = \frac{\tilde{N} - \tilde{N}_\infty}{\tilde{N}_w - \tilde{N}_\infty}. \end{aligned} \tag{7}$$

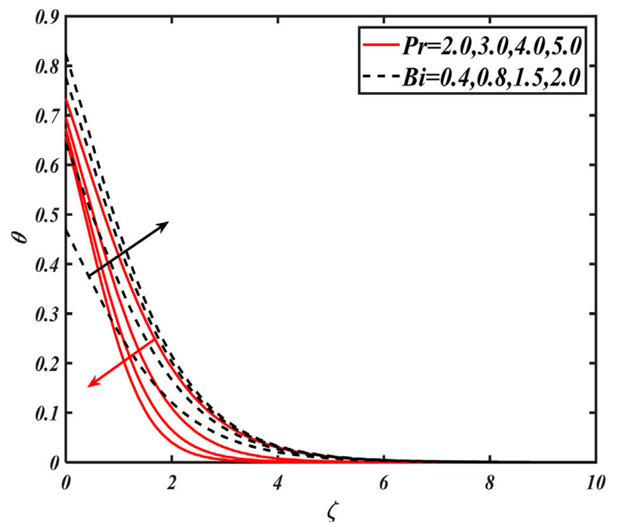

FIGURE 5
Illustration of Pr and Bi on θ.

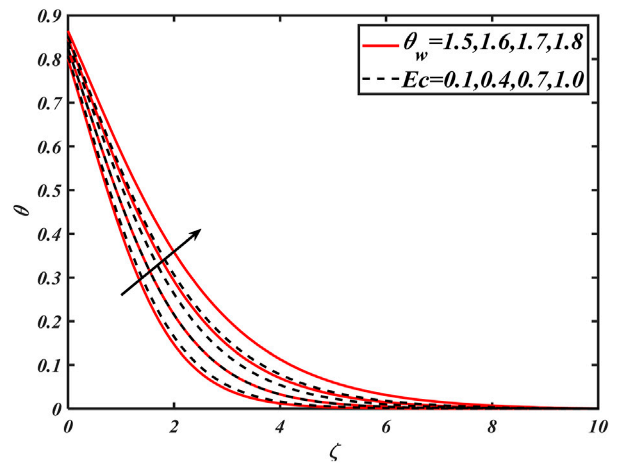

FIGURE 6
Illustration of θ_w and Ec on θ.

The governing equations with the aforementioned variables yield these Equations 8–12 in dimensionless forms:

$$(1-s)f''' + f''f'''sW_e - f'^2 + ff''' - f'M + \lambda(\theta - Nr\phi - Rb\chi) = 0, \tag{8}$$

$$\theta''\frac{1}{P_r} + f\theta' + (1+\theta(\theta_w-1))^2\left(\left(\theta(\theta_w-1) + 3\theta'^2(\theta_w-1)+1\right)\theta''\right)\frac{R}{P_r} + (1-s)Ecf''^2\frac{s}{2}WeEc\left(f''\right)^3 + \theta'^2Nt + \theta'\phi'Nb + f'^2MEc = 0, \tag{9}$$

$$\phi'' + \frac{Nt}{Nb}\theta'' + \phi'Scf - \phi\, exp\left[\frac{-E}{1+\delta\theta}\right]Sc\sigma_1{}^2(1+\delta\theta)^n = 0, \tag{10}$$

$$\chi'' + \chi'Lbf - Pe\left(\chi'\phi' + \phi''(\chi+\delta_1)\right) = 0, \tag{11}$$

with

$$\begin{aligned}&f'(\infty)\to 0, f(0)=0, f'(0)=1, \theta(\infty)\to 0, \theta(0)=1,\\ &\phi(\infty)\to 0, \phi(0)=1, \chi(0)=1, \chi(\infty)\to 0,\end{aligned} \tag{12}$$

where the Hartmann number is denoted by ($M = \frac{\sigma B_0{}^2}{\rho a}$), Prandtl number ($Pr = \frac{(\rho c_p)_f \nu}{k}$), ($R = \frac{16\sigma^* \tilde{T}_\infty^3}{3kk^*}$) shows the radiation parameter, ($W_e = \frac{a^{\frac{2}{3}}\sqrt{2}\,\Gamma U}{\sqrt{\nu}}$) represents the Weissenberg number, ($Ec = \frac{a^2U^2}{c_p(T_f - T_\infty)}$) is the Eckert number, ($\lambda = \frac{Gr}{Re_x^2}$) denotes the variable for mixed convection, temperature Grashof number, $Nr = (\frac{g\beta_c(C_w - C_\infty)}{g\beta_T(T_w - T_\infty)})$ is the buoyancy force, $Rb = (\frac{\gamma_1(\rho_m - \rho_f)(N_w - N_\infty)}{\rho_f\beta(1-C_\infty)(T_w - T_\infty)})$ is the bioconvection Rayleigh number, the Schmidt number is represented by ($Sc = \frac{\nu}{D_B}$), the chemical reaction rate constant is ($\sigma_1 = \frac{k_r^2}{a}$), ($\delta = \frac{\tilde{T}_w - \tilde{T}_\infty}{\tilde{T}_\infty}$) is the temperature relative parameter, ($\upsilon = \frac{E_a}{\kappa\tilde{T}_\infty}$) represents the activation energy parameter, ($Nt = \frac{(\rho c_p)_s D_T(\tilde{T}_w - \tilde{T}_\infty)}{\tilde{T}_\infty(\rho c_p)_f \nu}$) is the parameter for the thermophoresis effect, ($Nb = \frac{(\rho c_p)_s D_T(\tilde{C}_w - \tilde{C}_\infty)}{\tilde{T}_\infty \nu(\rho c_p)_f}$) is the Brownian motion parameter, (Lb) is the bioconvection Lewis parameter, ($Pe = \frac{bW_c}{D_m}$) shows the Peclet number, ($\delta_1 = \frac{\tilde{N}_\infty}{\tilde{N}_w - \tilde{N}_\infty}$) is the motile microorganism difference parameter, and ($\theta_w = \frac{\tilde{T}_w}{\tilde{T}_\infty}$) is the temperature ratio parameter.

The following are the mathematical expressions (Equations 13–16) for the motile density number, local Sherwood number, skin friction coefficient, and the local Nusselt number:

$$\begin{aligned}&C_f = \frac{2\tau_w}{\rho U_w{}^2}, Nu_x = \frac{xq_w}{k\left(\tilde{T}_w - \tilde{T}_\infty\right)}, Sh_x = \frac{xq_m}{k\left(\tilde{C}_w - \tilde{C}_\infty\right)},\\ &Nn_x = \frac{xq_n}{k\left(\tilde{N}_w - \tilde{N}_\infty\right)},\end{aligned} \tag{13}$$

with

$$\begin{aligned}&\tau_w\mu(1-s)\left(\frac{\partial\tilde{u}_1}{\partial y}\right)_{y=0} + \mu\frac{s\Gamma}{\sqrt{2}}\left(\frac{\partial\tilde{u}_1}{\partial y}\right)^3_{y=0}, q_w = -\left(\frac{\partial\tilde{T}}{\partial y}\right)_{y=0}k + (q_r)_w,\\ &q_m = -\left(\frac{\partial\tilde{C}}{\partial y}\right)_{y=0}D_B, q_n = -\left(\frac{\partial\tilde{N}}{\partial y}\right)_{y=0}D_m,\end{aligned} \tag{14}$$

where

$$(q_r)_w = \frac{-16\sigma^*\tilde{T}^3}{3k^*}\left(\frac{\partial\tilde{T}}{\partial y}\right)_{y=0}. \tag{15}$$

The above quantities are expressed as follows in non-dimensional forms:

$$\begin{aligned}&\frac{1}{2}Re^{\frac{1}{2}}C_f = f''(0)(1-s) + \frac{sWe}{2}\left(f''(0)\right)^2, Nu_xRe^{-0.5}\\ &= -\theta'(0)\left[1 + R\theta_w^3\right], Sh_xRe^{-0.5} = -\phi'(0), Nn_xRe^{-0.5}\\ &= -\chi'(0),\end{aligned} \tag{16}$$

where C_f, Nu, Sh, Nn, and R_{ex} are the coefficients of skin friction, the local Sherwood, the local Nusselt, the Reynolds number ($Re_x = \frac{a^2x}{\nu}$), and motile density, respectively.

3 Entropy generation

For tangent hyperbolic fluid, entropy generation is [58]

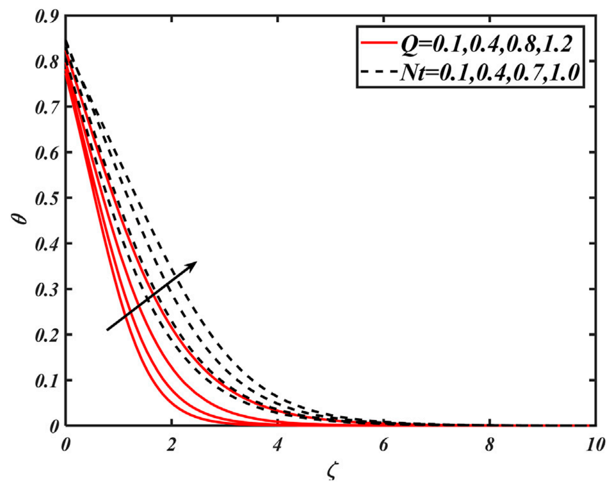

FIGURE 7
Illustration of Q and Nt on θ.

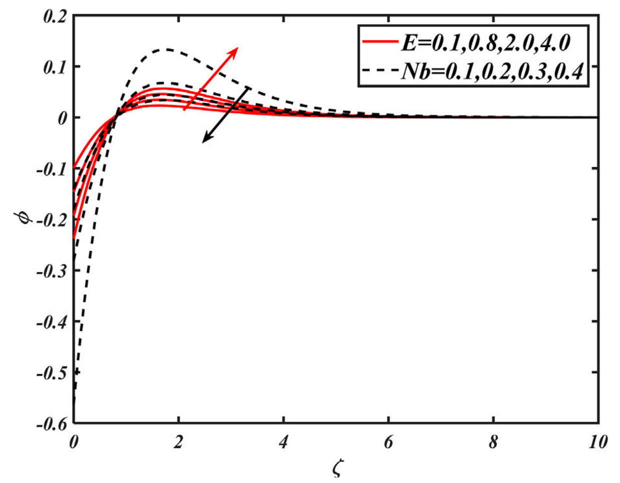

FIGURE 9
Illustration of PeE and Nb on ϕ.

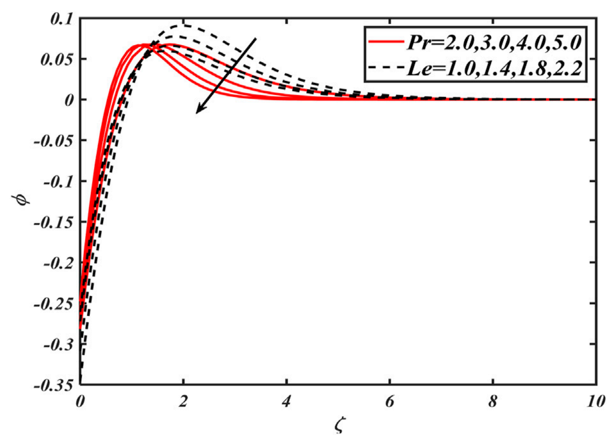

FIGURE 8
Illustration of Pr and Le on ϕ.

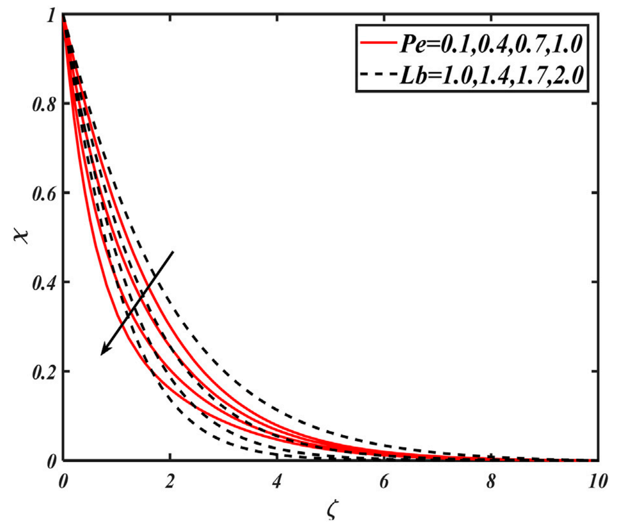

FIGURE 10
Illustration of Pe and Lb on χ.

$$\left.S_G = \underbrace{\frac{k}{\tilde{T}_\infty^2}\left[1+\frac{16\sigma^*\tilde{T}^3}{3kk^*}\right]}_{\text{Thermal irreversibility}} + \underbrace{\frac{\mu}{\tilde{T}_\infty}\Phi}_{\text{Fluid Friction irreversibility}} + \underbrace{\frac{\sigma}{\tilde{\tilde{T}}_\infty}B_0^2\left(u_1^2\right)}_{\text{Joule dissipation irreversibility}} + \underbrace{\frac{RD}{\tilde{T}_\infty}\left(\frac{\partial\tilde{T}}{\partial y}\frac{\partial\tilde{C}}{\partial y}\right) + \frac{RD}{\tilde{C}_\infty}\left(\frac{\partial\tilde{C}}{\partial y}\right)^2}_{\text{Concentration irreversibility}} + \underbrace{\frac{RD}{\tilde{N}_\infty}\left(\frac{\partial\tilde{N}}{\partial y}\right)^2 + \frac{RD}{\tilde{T}_\infty}\left(\frac{\partial\tilde{N}}{\partial y}\frac{\partial\tilde{T}}{\partial y}\right)}_{\text{Microorganisms concentration irreversibility}},\right\} \tag{17}$$

where

$$\Phi = \left(\frac{\partial u_1}{\partial y}\right)^2(1-s) + \frac{s\Gamma}{\sqrt{2}}\left(\frac{\partial u_1}{\partial y}\right)\left(\frac{\partial u_1}{\partial y}\right)^2. \tag{18}$$

Now Equation 17 becomes using Equation 18

$$\left.S_G = \underbrace{\frac{k}{\tilde{T}_\infty^2}\left[1+\frac{16\sigma^*\tilde{T}^3}{3kk^*}\right]}_{\text{Thermal irreversibility}} + \underbrace{\frac{\mu}{\tilde{T}_\infty}\left[(1-s)\left(\frac{\partial u_1}{\partial y}\right)^2 + \frac{s\Gamma}{\sqrt{2}}\left(\frac{\partial u_1}{\partial y}\right)\left(\frac{\partial u_1}{\partial y}\right)\right]}_{\text{Fluid Friction irreversibility}} + \underbrace{\frac{\sigma}{\tilde{\tilde{T}}_\infty}B_0^2\left(u_1^2\right)}_{\text{Joule dissipation irreversibility}} + \underbrace{\frac{RD}{\tilde{C}_\infty}\left(\frac{\partial\tilde{C}}{\partial y}\right)^2 + \left(\frac{\partial\tilde{C}}{\partial y}\frac{\partial\tilde{T}}{\partial y}\right)\frac{RD}{\tilde{T}_\infty}}_{\text{Nanoparticle concentration irreversibility}} + \underbrace{\left(\frac{\partial\tilde{N}}{\partial y}\right)^2\frac{RD}{\tilde{N}_\infty} + \frac{RD}{\tilde{T}_\infty}\left(\frac{\partial\tilde{T}}{\partial y}\frac{\partial\tilde{N}}{\partial y}\right)}_{\text{Microorganisms concentration irreversibility}}.\right\} \tag{19}$$

Equation 19 contains five factors: i) viscosity dissipation in the entropy generation for tangent hyperbolic fluid, ii) thermal irreversibility, iii) nanoparticle concentration irreversibility, iv) Joule effect irreversibility, and v) microorganism concentration irreversibility. The dimensionless form are in Equation 20

$$\left.\begin{aligned} N_g &= \left[R\left(\theta\left(\theta_w-1\right)+1\right)^3+1\right]\alpha_1\theta'^2 + (1-s)f''^2 Br + \left(f''\right)^3 Br\frac{We}{2} \\ &+ BMrf'^2 + L\frac{\alpha_2}{\alpha_1}\phi'^2 + L\theta'\phi' + L^*\frac{\alpha_3}{\alpha_1}\chi'^2 + L^*\theta'\chi',\end{aligned}\right\} \tag{20}$$

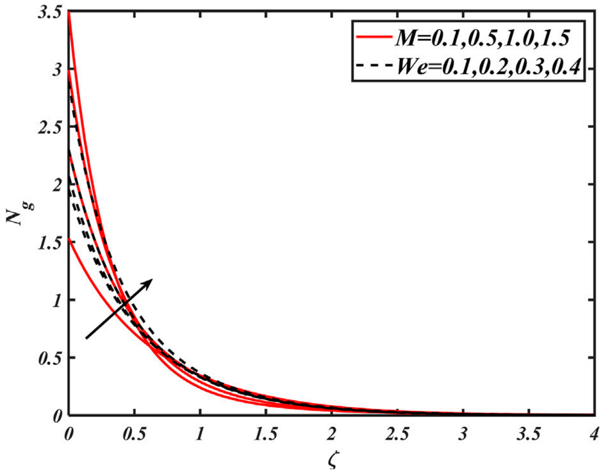

FIGURE 11
Illustration of M and We on N_g.

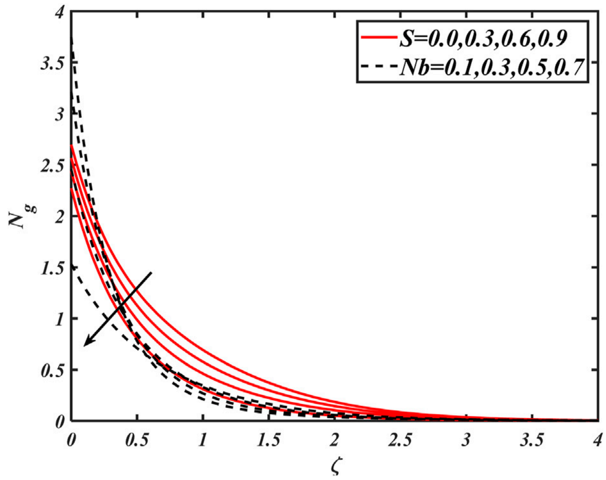

FIGURE 12
Illustration of S and Nb on N_g.

$$\left.\begin{aligned}&\alpha_1 = \frac{\Delta\tilde{T}}{\tilde{T}_\infty} = \frac{\tilde{T}_w - \tilde{T}_\infty}{\tilde{T}_\infty}, \alpha_2 = \frac{\Delta\tilde{C}}{\tilde{C}_\infty} = \frac{\tilde{C}_w - \tilde{C}_\infty}{\tilde{C}_\infty}, \alpha_3 = \frac{\tilde{N}_w - \tilde{N}_\infty}{\tilde{N}_\infty} = \frac{\Delta\tilde{N}}{\tilde{N}_\infty},\\ &Br = \frac{\mu a^2}{k\Delta\tilde{T}}, N_g = \frac{\tilde{T}_\infty S_G \nu}{ak\Delta\tilde{T}}, L = \frac{RD\left(\tilde{C}_w - \tilde{C}_\infty\right)}{k},\\ &L^* = \frac{RD\left(\tilde{N}_w - \tilde{N}_\infty\right)}{k},\end{aligned}\right\} \tag{21}$$

where Equation 21 represents $\alpha_1, \alpha_2, \alpha_3, Br, L, L^*, \text{and}\, N_g$ differences in the temperature variable, Brinkman number, concentration difference parameter, diffusion parameter due to nanoparticles and microorganisms' concentration, and local entropy generation. The dimensionless Bejan number is expressed in Equation 22 and mathematical form is in Equation 23

$$Be = \frac{\text{Entropy generation due to mass and heat transfer}}{\text{Total entropy generation}}, \tag{22}$$

$$\left.Be = \frac{\left[1 + R(\theta(\theta_w - 1) + 1)^3\right]\theta'^2\alpha_1 L\theta'\phi' + L\frac{\alpha_2}{\alpha_1}\phi'^2 + L\theta'\phi' + L^*\frac{\alpha_3}{\alpha_1}\chi'^2 + L^*\theta'\chi'}{(1-s)Brf''^2 + \left[1 + R(\theta(\theta_w - 1) + 1)^3\right]\theta'^2\alpha_1 + \frac{We}{2}(f'')^3 Br + BMrf'^2 + \frac{\alpha_2}{\alpha_1}L\phi'^2 + \theta'\phi' L + L^*\frac{\alpha_3}{\alpha_1}\chi'^2 + L^*\theta'\chi'}\right\}. \tag{23}$$

$$f = z_1, f' = z_2, f'' = z_3, f'' = z_3', \theta = z_4, \theta' = z_5, \theta'' = z_5',$$
$$\phi = z_6, \phi' = z_7, \phi'' = z_7', \chi = z_8, \chi' = z_9, \chi'' = z_9'.$$

Then,

$$z_3' = \frac{\left[z_2^2 - z_1 z_3 + Mz_2 - \lambda z_4\left(1 + \beta_t z_4\right) - \lambda z_6 N^*\left(1 + \beta_c z_6\right) - \lambda z_8 N^{**}\left(1 + \beta_n z_8\right)\right]}{(1 - s + sWez_3)}, \tag{24}$$

$$z_5' = \frac{\begin{bmatrix} -3R\left(z_4\left(\theta_w - 1\right) + 1\right)^2\left(z_5^2\left(\theta_w - 1\right)\right) - Pr\, z_1 z_5 - (1-s)Ec^2 z_3^5\frac{s}{2}WePr \\ -NtPrz_5^2 - NbPrz_5 z_7 - Mz_2^2 EcPr\end{bmatrix}}{\left[1 + R\left(z_4\left(\theta_w - 1\right) + 1\right)^2\left(z_4\left(\theta_w - 1\right) + 1\right)\right]}, \tag{25}$$

$$z_7' = -\frac{Nt}{Nb}z_5' - Scz_1 z_7 + Sc\sigma_1^2\left(1 + \delta z_4\right)^n exp\left[\frac{-\upsilon}{1 + \delta z_4}\right]z_6, \tag{26}$$

$$z_9' = -Lbz_1 z_9 + Pe\left[z_7'\left(z_8 + \delta_1\right) + z_7 z_9\right]. \tag{27}$$

The transformed boundary conditions are

$$\begin{aligned}&z_1(0) = 0, z_2(\infty) \to 0, -1 + z_2(0) = 0, -1 + z_4(0) = 0, z_4(\infty) \to 0,\\ &z_6(0) - 1 = 0, z_6(\infty) \to 0, z_8(0) - 1 = 0, z_8(\infty) \to 0.\end{aligned} \tag{28}$$

4 Numerical algorithm

It is a well-known observation that a number of physical models contain differential equations which are nonlinear depending on the included constraints that can be solved using numerical approaches. In the suggested numerical approaches, the shooting method is perhaps a more reliable strategy for achieving adequate accuracy. After generating dimensionless forms, the bvp4c built-in package is used to tackle numerically. This approach is reliable and efficient, having an error tolerance of 10^{-6}. As a result, we used this strategy to target Equations 8–12. The collection of these mathematical equations is turned into first-order differential equations using dummy variables as in Equations 24–28:

5 Discussion

This part describes the visual representation of physical characteristics such as velocity distribution f', temperature θ, nanoparticle concentration ϕ, and motile gyrotactic χ. In the process of modifying the related physical parameter, the quantities that are left have been allotted constant values such as $M = 0.5, s = \lambda = \beta_c = We = \sigma_1 = \delta = Ec = 0.1, Sc = Nb = Nt = N^* = 0.01,$ $\Pr = 2,$ and $\theta_w = 1.1.$ Figures 2–4 examine the behavior of a variety of physical factors, including the Hartmann number M, Weissenberg number We, first-order velocity slip α, buoyancy ratio parameter Nr, second-order slip parameter β, and mixed convection variable λ. The effects of the Hartmann number M and We Weissenberg number on the velocity

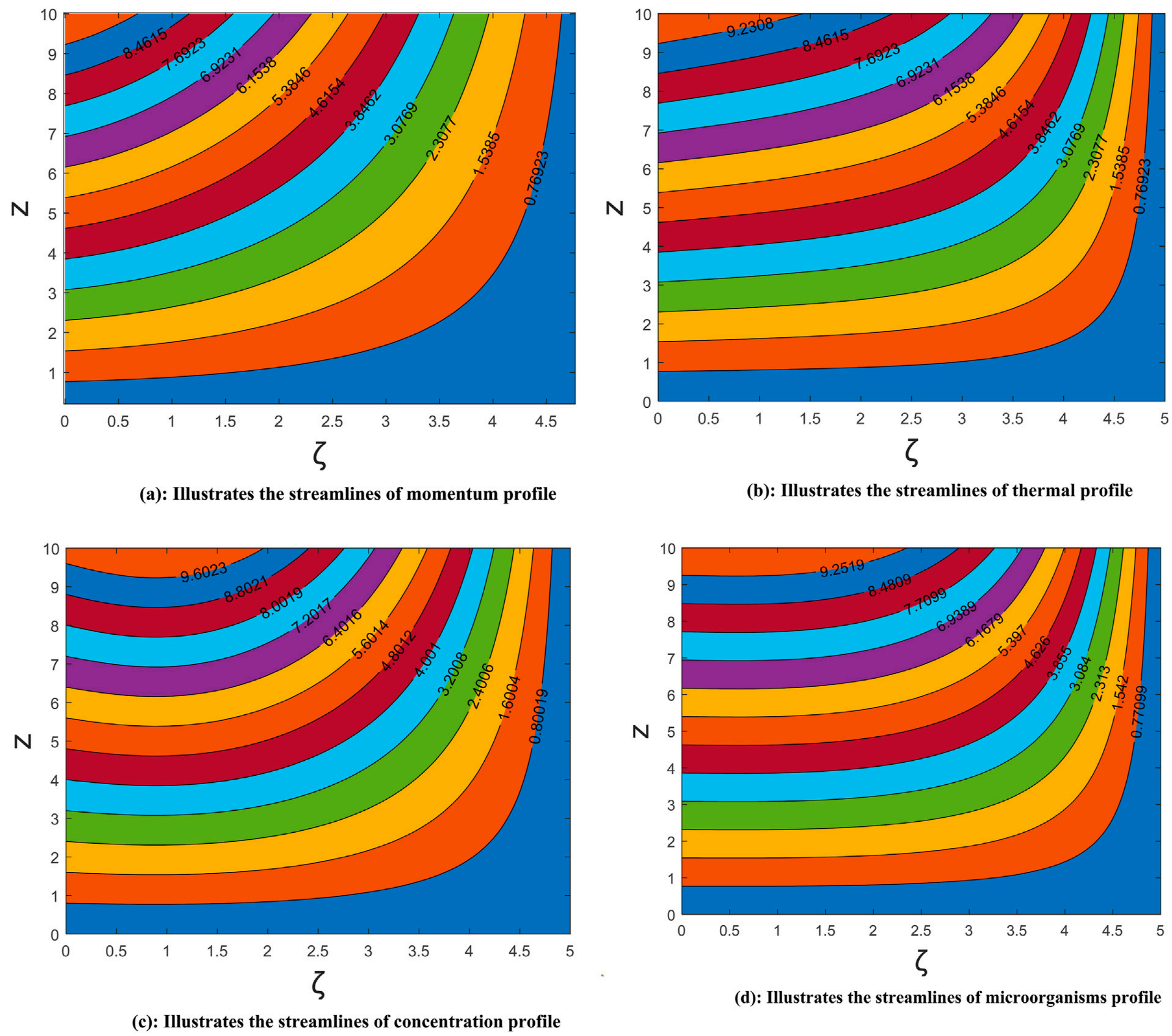

FIGURE 13
(A) Streamlines of the momentum profile. **(B)** Streamlines of the thermal profile. **(C)** Streamlines of the concentration profile. **(D)** Streamlines of the microorganism profile.

TABLE 1 Comparison of $f⋑(0)$ with available results.

M	Ref. [2]	Ref. [5]	Ref. [57]	Present
0.0	−1.000	−1.000	−1.000	−1.000
0.5	−1.18034	−1.1803	−1.18034	−1.18033
1.0	−1.414214	−1.41421	−1.414214	−1.414215

graph f' are depicted in Figure 2. A declining behavior is prominent for velocity distribution by increasing both M and We. For higher values of (M = 0.1, 0.4, 8, 1.2), Figure 2 shows a decreasing trend of $f'(\xi)$. Because M depends on the Lorentz force, the inter-particle resistance increases as M increases, which reduces $f'(\xi)$. We observe that as We increases, fluid motion gradually decreases. Given that the fraction of relaxation time by a particular processing time is denoted by We, larger We will give rise to a longer relaxation period, which will lessen the velocity profile. Figure 3 discusses the first-order slip parameter α. In addition, the mixed convection parameter λ for the profile of velocity $f'(\xi)$. First, it should be noted that the first order is the feature of the medium that is linked to the pathways between fluid flows. The values for the velocity declines as we change first-order slip parameters. Moreover, it is noticed that the thickness of the boundary, which is entitled to first-order slip factor, is decreasing. The velocity profile increases with the increase in the mixed convection parameter λ. Physically, the buoyant force overcomes the force, owing to the increase in inertia as the parameter for mixed convection, and as a result, a leading increase is noticed for $f'(\xi)$.

The parameter for the buoyancy ratio Nr and the parameter for the second-order slip β for the dimensionless distribution of velocity $f'(\xi)$ are graphed in Figure 4. The profile for velocity decreases as both of these factors increase.

The impacts of the Prandtl number Pr, Biot number Bi, heat sink/source Q, parameter for thermophoresis Nt, temperature ratio parameter θ_w, and Eckert number Ec on θ temperature field are depicted in Figures 5–7. Figure 5 shows the physical impact caused by Pr and Bi on temperature field θ. It is easy to observe that θ is the decreasing function of (Pr = 2.0, 3.0, 4.0, 5.0). Furthermore, the thermal Biot number Bi has a connection to the coefficient of heat transfer that causes the increase in the temperature distribution of nanoparticles. The Eckert number Ec and the characteristics of parameters for the temperature ratio θ_w and on the profile for temperature θ are demonstrated in Figure 6. In fluid temperature θ, an increasing trend is prominent for the increase in the values of parameters for the temperature ratio (θ_w = 1.5, 1.6, 1.7, 1.8). For increasing values of Ec, it displays that the fluid temperature shows an increase. The reason for it being higher Ec fluid friction results in an interconversion of mechanical energy and thermal energy, which peaks the temperature θ of the fluid.

The effects of the $(Q < 0)$ heat sink or $(Q > 0)$ heat source and thermophoresis parameter Nt are shown in Figure 7. In the boundary layer, when a heat source is present, it increases energy, which results in the increase in fluid's temperature. The existence of a heat sink in the boundary layer absorbs energy, which, in turn, lowers the temperature of the fluid. These behaviors are depicted in Figure 7. For larger Nt, particles of fluid increase from hot to cold areas of the system. The temperature profile increases as a result of an increase in thermophoresis force.

To examine the changes in concentration distribution ϕ versus different values of the E activation energy, Pr Prandtl number, Le Lewis number, and Nb Brownian movement, Figures 8, 9 are formulated. Figure 8 presents the graph of the Prandtl number Pr and Lewis number Le on ϕ. Increases in Pr and Le result in decreases in the profile of concentration of nanoparticles. The ramifications of yet two other crucial parameters, the parameters for Brownian motion Nb and activation energy E, are shown in Figure 9. Although the concentration of nanoparticles decreases with Nb, but for E, the profile for the concentration improves.

The *Peclet number* Pe and Lewis number Lb for bioconvection effects on the self-propelled microorganism profile χ are shown in Figure 10. By altering Pe, a retarding behavior is discovered; this tendency establishes because Pe develops a reverse relationship with microorganism diffusivity. χ reduced as a result of this inverse relationship. A distinguishing motile microorganism profile is found when the value of Lb increases. The physical reasoning is that a bigger change in Lb is connected with the reduced diffusion of self-propelled microorganisms, and χ decays as a result of this. Figures 11, 12 examine the behavior of a variety of physical factors, including the Hartmann number M, power law index s, and Nb parameters for Brownian motion on entropy generation N_g. Salient features of the Hartmann number M and Weissenberg number We for entropy generation N_g are displayed in Figure 11. The increase in resistance for increasing M entropy generation shows an increasing trend. Relaxation time increases for higher We, which indicates increased heat loss due to increased resistance between liquid particles. Consequently, entropy generation increases. Figure 12 is plotted to examine the entropy generation for greater values of s, which is the power law index and Brownian motion parameter Nb. For the increase in s and Nb, entropy generation N_g shows decreasing behavior.

6 Streamlines

The streamlines of the flow problem visualize the flow pattern and movement of the molecules, as displayed in Figures 13A–D. The laminar pattern is visible among all profiles, and no intersection is found. These streamlines describe the movement, velocity distribution, heat transport efficiency, and interaction with the surface body.

7 Tables

In the tabulated values in Table 1, we see the comparison of our computed results with the already in the tabulated values we see the comparison of our computed results with the already results shows the great accord with available literature.

8 Conclusion

The aim of this contribution is to study the flow of tangent hyperbolic nanomaterials for entropy optimization, owing to a stretchable surface. Some key findings are as follows:

- For the first-order velocity slip factor, the velocity distribution increases, but the Hartmann number, Weissenberg number, buoyancy ratio constant, and second-order slip parameter show a declining trend.
- The thermal Biot number, parameter for the temperature ratio, Eckert number, and parameter for thermophoresis enhanced the temperature of nanoparticles, while a decreasing trend is noticed for the Prandtl number.
- Activation energy improved the concentration of nanoparticles, while it reduces the concentration for the Prandtl number, Lewis number, and Brownian parameter.
- The distribution for self-propelling gyrotactic microorganisms declines for larger Lewis and Prandtl numbers.
- Entropy generation reduces for a larger power law index and parameters for Brownian motion; however, a negative relationship is observed for larger Weissenberg and Hartmann numbers.

In the future, this approach may be extended to include the various heat and mass flux models, as well as the observation of changes in transport rates due to geometrical changes.

Data availability statement

The original contributions presented in the study are included in the article/Supplementary Material; further inquiries can be directed to the corresponding author.

Author contributions

YW: writing–review and editing and methodology. MC: conceptualization and writing–original draft. NM: software and writing–original draft. MT: data curation and writing–original draft. MB: validation and writing–review and editing. MI: supervision and writing–original draft.

Funding

The author(s) declare that financial support was received for the research, authorship, and/or publication of this article. This research project is supported by the 2022 university-level scientific research team project, 2018 university-level quality engineering project, and 2023 Project of Natural Science Foundation of Colleges and Universities in Anhui Province (kytd202207; 2018jpkcx17; and 2023AH030085).

Conflict of interest

The authors declare that the research was conducted in the absence of any commercial or financial relationships that could be construed as a potential conflict of interest.

References

1. Malik MY, Salahuddin T, Hussain A, Bilal S. MHD flow of tangent hyperbolic fluid over a stretching cylinder: using Keller box method. *J Magnetism Magn Mater* (2015) 395:271–6. doi:10.1016/j.jmmm.2015.07.097

2. Waqas M, Khan MI, Hayat T, Alsaedi A, Khan MI. Nonlinear thermal radiation in flow induced by a slendering surface accounting thermophoresis and Brownian diffusion. *The Eur Phys J Plus* (2017) 132(6):280–13. doi:10.1140/epjp/i2017-11555-0

3. Akbar NS, Nadeem S, Haq RU, Khan ZH. Numerical solutions of magnetohydrodynamic boundary layer flow of tangent hyperbolic fluid towards a stretching sheet. *Indian J Phys* (2013) 87(11):1121–4. doi:10.1007/s12648-013-0339-8

4. Nadeem S, Akbar NS. Series solutions for the peristaltic flow of a Tangent hyperbolic fluid in a uniform inclined tube. *Z Fr Naturforschung A* (2010) 65(11): 887–95. doi:10.1515/zna-2010-1101

5. Hayat T, Khan MI, Waqas M, Alsaedi A. Stagnation point flow of hyperbolic tangent fluid with Soret-Dufour effects. *Results Phys* (2017) 7:2711–7. doi:10.1016/j.rinp.2017.07.014

6. Waqas M, Farooq M, Khan MI, Alsaedi A, Hayat T, Yasmeen T. Magnetohydrodynamic (MHD) mixed convection flow of micropolar liquid due to nonlinear stretched sheet with convective condition. *Int J Heat Mass Transfer* (2016) 102:766–72. doi:10.1016/j.ijheatmasstransfer.2016.05.142

7. Hayat T, Khan MI, Waqas M, Alsaedi A. Effectiveness of magnetic nanoparticles in radiative flow of Eyring-Powell fluid. *J Mol Liquids* (2017) 231:126–33. doi:10.1016/j.molliq.2017.01.076

8. Hayat T, Waqas M, Khan MI, Alsaedi A, Shehzad SA. Magnetohydrodynamic flow of burgers fluid with heat source and power law heat flux. *Chin J Phys* (2017) 55(2): 318–30. doi:10.1016/j.cjph.2017.02.004

9. Hayat T, Qasim M, Abbas Z. Radiation and mass transfer effects on the magnetohydrodynamic unsteady flow induced by a stretching sheet. *Z fr Naturforschung A* (2010) 65(3):231–9. doi:10.1515/zna-2010-0312

10. Sheikholeslami M, Zeeshan A. Numerical simulation of Fe3O4-water nanofluid flow in a non-Darcy porous media. *Int J Numer Methods Heat and Fluid Flow* (2018) 28(3):641–60. doi:10.1108/hff-04-2017-0160

11. Khan MI, Waqas M, Hayat T, Alsaedi A. A comparative study of Casson fluid with homogeneous-heterogeneous reactions. *J Colloid Interf Sci* (2017) 498:85–90. doi:10.1016/j.jcis.2017.03.024

12. Zeeshan A, Shehzad N, Ellahi R. Analysis of activation energy in Couette-Poiseuille flow of nanofluid in the presence of chemical reaction and convective boundary conditions. *Results Phys* (2018) 8:502–12. doi:10.1016/j.rinp.2017.12.024

13. Hassan M, Zeeshan A, Majeed A, Ellahi R. Particle shape effects on ferrofuids flow and heat transfer under influence of low oscillating magnetic field. *J Magnetism Magn Mater* (2017) 443:36–44. doi:10.1016/j.jmmm.2017.07.024

14. Hayat T, Khan MI, Qayyum S, Alsaedi A. Entropy generation in flow with silver and copper nanoparticles. Colloids and Surfaces A. *Physicochemical Eng Aspects* (2018) 539:335–46. doi:10.1016/j.colsurfa.2017.12.021

15. Hayat T, Qayyum S, Khan MI, Alsaedi A. Entropy generation in magnetohydrodynamic radiative flow due to rotating disk in presence of viscous dissipation and Joule heating. *Phys Fluids* (2018) 30(1):1070–6631. doi:10.1063/1.5009611

16. Rashidi S, Akar S, Bovand M, Ellahi R. Volume of fluid model to simulate the nanofluid flow and entropy generation in a single slope solar still. *Renew Energ* (2018) 115:400–10. doi:10.1016/j.renene.2017.08.059

17. Kuznetsov AV, Avramenko AA. Effect of small particles on this stability of bioconvection in a suspension of gyrotactic microorganisms in a layer of finite depth. *Int Commun Heat Mass Transfer* (2004) 31(1):1–10. doi:10.1016/s0735-1933(03)00196-9

18. Geng P, Kuznetsov AV. Settling of bidispersed small solid particles in a dilute suspension containing gyrotactic micro-organisms. *Int J Eng Sci* (2005) 43(11-12): 992–1010. doi:10.1016/j.ijengsci.2005.03.002

19. Kuznetsov AV. Non-oscillatory and oscillatory nanofluid bio-thermal convection in a horizontal layer of finite depth. *Eur J Mechanics-B/Fluids* (2011) 30(2):156–65. doi:10.1016/j.euromechflu.2010.10.007

20. Bég OA, Prasad VR, Vasu B. Numerical study of mixed bioconvection in porous media saturated with nanofluid containing oxytactic microorganisms. *J Mech Med Biol* (2013) 13(04):1350067. doi:10.1142/s021951941350067x

21. Akbar NS. Bioconvection peristaltic flow in an asymmetric channel filled by nanofluid containing gyrotactic microorganism. *Int J Numer Methods Heat and Fluid Flow* (2015) 25(2):214–24. doi:10.1108/hff-07-2013-0242

22. Bhatti MM, Zeeshan A, Ellahi R. Simultaneous effects of coagulation and variable magnetic field on peristaltically induced motion of Jeffrey nanofluid containing gyrotactic microorganism. *Microvasc Res* (2017) 110:32–42. doi:10.1016/j.mvr.2016.11.007

23. Abbas IA, Palani G. Effects of magnetohydrodynamic flow past a vertical plate with variable surface temperature. *Appl Maths Mech* (2010) 31(3):329–38. doi:10.1007/s10483-010-0306-9

24. Chakraborty T, Das K, Kundu PK. Framing the impact of external magnetic field on bioconvection of a nanofluid flow containing gyrotactic microorganisms with convective boundary conditions. *Alexandria Eng J* (2018) 57(1):61–71. doi:10.1016/j.aej.2016.11.011

25. Choi SUS, Zhang ZG, Yu W, Lockwood FE, Grulke EA. Anomalous thermal conductivity enhancement in nanotube suspensions. *Appl Phys Lett* (2001) 79(14): 2252–4. doi:10.1063/1.1408272

26. Li S, Faizan M, Ali F, Ramasekhar G, Muhammad T, Khalifa HAEW, et al. Modelling and analysis of heat transfer in MHD stagnation point flow of Maxwell nanofluid over a porous rotating disk. *Alexandria Eng J* (2024) 91:237–48. doi:10.1016/j.aej.2024.02.002

27. Reddy MV, Ajithkumar M, Lone SA, Ali F, Lakshminarayana P, Saeed A. Magneto-Williamson nanofluid flow past a wedge with activation energy: Buongiorno model. *Adv Mech Eng* (2024) 16(1):16878132231223027. doi:10.1177/16878132231223027

28. Ali F, Zaib A, Faizan M, Zafar SS, Alkarni S, Shah NA, et al. Heat and mass exchanger analysis for Ree-Eyring hybrid nanofluid through a stretching sheet utilizing the homotopy perturbation method. *Case Stud Therm Eng* (2024) 54:104014. doi:10.1016/j.csite.2024.104014

29. Ali F, Mahnashi AM, Hamali W, Raizah Z, Saeed A, Khan A. Numerical scrutinization of Darcy–Forchheimer flow for trihybrid nanofluid comprising of (GO+ZrO2+SiO2/kerosene oil) over the curved surface. *J Therm Anal Calorim* (2024) 1–16. doi:10.1007/s10973-024-13103-w

30. Yasmin H, Lone SA, Ali F, Alrabaiah H, Raizah Z, Saeed A. Thermal radiative flow of cross nanofluid due to a stretched cylinder containing microorganisms. *Nanotechnology Rev* (2023) 12(1):20230147. doi:10.1515/ntrev-2023-0147

31. Vinodkumar Reddy M, Ajithkumar M, Zafar SSB, Faizan M, Ali F, Lakshminarayana P. Magnetohydrodynamic stagnation point flow of Williamson hybrid nanofluid via stretching sheet in a porous medium with heat source and chemical reaction. *Proc Inst Mech Eng E: J Process Mech Eng* (2024): 09544089241239583. doi:10.1177/09544089241239583

32. Ahmed MF, Ali F, Zafar SS, Reddy CS, Aslam M. Irreversibility analysis and thermal radiative of Williamson (ZnO+MOS2/C3H8O2) hybrid nanofluid over a porous surface with a suction effect. *Physica Scripta* (2023) 98(11):115237. doi:10.1088/1402-4896/acffff

33. Lone SA, Ali F, Saeed A, Bognár G. Irreversibility analysis with hybrid cross nanofluid of stagnation point and radiative flow (TiO2+CuO) based on engine oil past a stretchable sheet. *Heliyon* (2023) 9(4):e15056. doi:10.1016/j.heliyon.2023.e15056

34. Zhang T, Khan SU, Imran M, Tlili I, Waqas H, Ali N. Activation energy and thermal radiation aspects in bioconvection flow of rate-type nanoparticles configured by a stretching/shrinking disk. *J Energ Resour Technol* (2020) 142(11):112102. doi:10.1115/1.4047249

35. Alghamdi M. Significance of Arrhenius activation energy and binary chemical reaction in mixed convection flow of nanofluid due to a rotating disk. *Coatings* (2020) 10(1):86. doi:10.3390/coatings10010086

36. Asma M, Othman WAM, Muhammad T. Numerical study for Darcy-Forchheimer flow of nanofluid due to a rotating disk with binary chemical reaction and Arrhenius activation energy. *Mathematics* (2019) 7(10):921. doi:10.3390/math7100921

37. Khan WA, Rashad AM, Abdou MMM, Tlili I. Natural bioconvection flow of a nanofluid containing gyrotactic microorganisms about a truncated cone. *Eur J Mechanics-B/Fluids* (2019) 75:133–42. doi:10.1016/j.euromechflu.2019.01.002

38. Rashad AM, Nabwey HA. Gyrotactic mixed bioconvection flow of a nanofluid past a circular cylinder with convective boundary condition. *J Taiwan Inst Chem Eng* (2019) 99:9–17. doi:10.1016/j.jtice.2019.02.035

39. Nabwey HA, El-Kabeir SMM, Rashad AM, Abdou MMM. Gyrotactic microorganisms mixed convection flow of nanofluid over a vertically surfaced saturated porous media. *Alexandria Eng J* (2022) 61(3):1804–22. doi:10.1016/j.aej.2021.06.080

40. Nabwey HA, A. Khan W, Rashad AM, Mabood F, Salah T. Power-law nanofluid flow over a stretchable surface due to gyrotactic microorganisms. *Mathematics* (2022) 10(18):3285. doi:10.3390/math10183285

41. Moatimid GM, Mohamed MA, Elagamy K. Heat and mass flux through a Reiner–Rivlin nanofluid flow past a spinning stretching disc: Cattaneo–Christov model. *Scientific Rep* (2022) 12(1):14468. doi:10.1038/s41598-022-18609-7

42. Moatimid GM, Mohamed MA, Elagamy K. A Casson nanofluid flow within the conical gap between rotating surfaces of a cone and a horizontal disc. *Scientific Rep* (2022) 12(1):11275. doi:10.1038/s41598-022-15094-w

43. Moatimid GM, Mohamed MA, Gaber AA, Mostafa DM. Numerical analysis for tangent-hyperbolic micropolar nanofluid flow over an extending layer through a permeable medium. *Scientific Rep* (2023) 13(1):13522. doi:10.1038/s41598-023-33554-9

44. Moatimid GM, Mohamed MA, Elagamy K. Peristaltic transport of Rabinowitsch nanofluid with moving microorganisms. *Scientific Rep* (2023) 13(1):1863. doi:10.1038/s41598-023-28967-5

45. He JH, Moatimid GM, Mohamed MA, Elagamy K. A stretching cylindrical carreau nanofluid border layer movement with motile microorganisms and variable thermal characteristics. *Int J Mod Phys B* (2023) 38:2450223. doi:10.1142/s0217979224502230

46. Moatimid GM, Mohamed MA, Elagamy K. A motion of Jeffrey nanofluid in porous medium with motile microorganisms between two revolving stretching discs: effects of Hall currents. *J Porous Media* (2022) 25(10):83–101. doi:10.1615/jpormedia.2022043529

47. Moatimid GM, Mohamed MA, Elagamy K. A pulsatile Williamson nanofluid flow with motile microorganisms between two permeable walls: effect of modified Darcy's law. *J Porous Media* (2023) 26(12):57–86. doi:10.1615/jpormedia.2023044143

48. Moatimid GM, Mohamed MA, Elagamy K. Microorganisms peristaltic transport within a Carreau Nanofluid through a modified Darcy porous medium. *Spec Top and Rev Porous Media: Int J* (2023) 14(5):1–30. doi:10.1615/specialtopicsrevporousmedia.2023046194

49. Moatimid GM, Mohamed MA, Elagamy K. A Williamson nanofluid with motile microorganisms across a vertical exponentially stretching porous sheet with varying thermal characteristics. *Spec Top and Rev Porous Media: Int J* (2024) 15(1):67–98. doi:10.1615/specialtopicsrevporousmedia.2023046440

50. Mohamed M, Elagamy K. Sutterby nanofluid flow with microorganisms around a curved expanding surface through a porous medium: thermal diffusion and diffusion thermo impacts. *J Porous Media* (2024) 27:19–48. doi:10.1615/JPorMedia.2024052470

51. Sheikholeslami M, Ganji DD. Influence of magnetic field on CuOH2O nanofluid flow considering Marangoni boundary layer. *Int J Hydrogen Energ* (2017) 42(5):2748–55. doi:10.1016/j.ijhydene.2016.09.121

52. Pandey AK, Kumar M. Boundary layer flow and heat transfer analysis on Cu-water nanofluid flow over a stretching cylinder with slip. *Alexandria Eng J* (2017) 56(4):671–7. doi:10.1016/j.aej.2017.01.017

53. Javed MF, Khan MI, Khan NB, Muhammad R, Rehman MU, Khan SW, et al. Axisymmetric flow of Casson fluid by a swirling cylinder. *Results Phys* (2018) 9:1250–5. doi:10.1016/j.rinp.2018.04.015

54. Khan NB, Ibrahim Z, Khan MI, Hayat T, Javed MF. VIV study of an elastically mounted cylinder having low mass-damping ratio using RANS model. *Int J Heat Mass Transfer* (2018) 121:309–14. doi:10.1016/j.ijheatmasstransfer.2017.12.109

55. Khan NB, Ibrahim Z, Bin Mohamad Badry AB, Jameel M, Javed MF. Numerical investigation of flow around cylinder at Reynolds number= 3900 with large eddy simulation technique: effect of spanwise length and mesh resolution. *J Eng Maritime Environ* (2019) 233(2):417–27. doi:10.1177/1475090217751326

56. Javed MF, Waqas M, Khan NB, Muhammad R, Rehman MU, Khan MI, et al. On entropy generation effectiveness in flow of power law fluid with cubic autocatalytic chemical reaction. *Appl Nanoscience* (2019) 9(5):1205–14. doi:10.1007/s13204-019-01064-8

57. Khan MI, Qayyum S, Hayat T, Khan MI, Alsaedi A, Khan TA. Entropy generation in radiative motion of tangent hyperbolic nanofluid in presence of activation energy and nonlinear mixed convection. *Phys Lett A* (2018) 382(31):2017–26. doi:10.1016/j.physleta.2018.05.021

58. Ahmed SE, Raizah ZAS, Aly AM. Entropy generation due to mixed convection over vertical permeable cylinders using nanofluids. *J King Saud University-Science* (2019) 31(3):352–61. doi:10.1016/j.jksus.2017.07.010

Nomenclature

Symbols of parameters

Description with SI units

x, y Cartesian coordinates $(-)$

D_m microorganism's diffusion coefficient $(-)$

$\tilde{u}_1, \tilde{u}_2$ velocity components (m/s)

Pr Prandtl number $(-)$

k nanofluid thermal conductivity $(W/m\ K)$

E_a activation energy variable $(-)$

C_f skin friction parameter $(-)$

C_∞ free stream concentration (mol/m^3)

k^* coefficient of mean absorption $(-)$

T_∞ ambient temperature (T)

D_B Brownian motion coefficient (m^2/s)

$\tilde{N}$ microorganism's density $(-)$

B_0 magnetic parameter $(Tesla)$

Sh_x local Sherwood number $(-)$

$\tilde{C}$ concentration of particles (mol/m^3)

Nb Brownian motion parameter $(-)$

Sc Schmidt number $(-)$

b chemotaxis constant $(-)$

$\tilde{T}$ temperature of particles (K)

M Hartmann number $(-)$

Nu_x local Nusselt number $(-)$

Pe Peclet number $(-)$

D_T thermophoresis coefficient (m^2/s)

$\tilde{C}_w$ surface concentration (mol/m^3)

$\tilde{T}_w$ surface temperature (T)

N_∞ ambient microorganisms $(-)$

Nt thermophoresis parameter $(-)$

W_e Weissenberg parameter $(-)$

R radiation parameter $(-)$

Lb bioconvection Lewis number $(-)$

Greek symbols

ρ_f density of the fluid (kg/m^3)

μ dynamic viscosity $(kg\,m^{-1}s^{-1})$

σ^* Stefan–Boltzmann constant $(-)$

α first-order slip parameter $(-)$

δ_1 motile microorganism difference parameter $(-)$

β second-order slip parameter $(-)$

λ mixed convection parameter $(-)$

ν kinematic viscosity (m^2/s)

θ_w temperature ratio parameter $(-)$

σ electrical conductivity (S/m)